BIOTECHNOLOGY
BIOENGINEERING WILEY

In vitro measurement of concentration of unlabeled protein within a hyaluronic acid matrix

Antonio C. F. dos Santos[1,2] [ID] | Adib Ahmadzadegan[3] | Eduardo Ximenes[1,2] |
Pavlos Vlachos[3,5] | Arezoo Ardekani[3] | Shiven Kapur[4] | Vince Corvari[4] |
Michael R. Ladisch[1,2,5] [ID]

[1]Laboratory of Renewable Resources Engineering, Purdue University, West Lafayette, Indiana, USA

[2]Department of Agricultural and Biological Engineering, Purdue University, West Lafayette, Indiana, USA

[3]School of Mechanical Engineering, Purdue University, West Lafayette, Indiana, USA

[4]Bioproduct Research and Development, Eli Lilly, Indianapolis, Indiana, USA

[5]Weldon School of Biomedical Engineering, Purdue University, West Lafayette, Indiana, USA

Correspondence
Michael R. Ladisch, Laboratory of Renewable Resources Engineering (LORRE), Purdue University, 225 S University St, West Lafayette, IN 47907-2093, USA.
Email: ladisch@purdue.edu

Abstract

There are currently more than 560 therapeutic monoclonal antibodies (mAbs) at various stages of research and clinical testing, including candidates for administration by subcutaneous (SC) injection. Preclinical studies based on in vitro measurements of high molecular weight proteins within simulated SC matrices are assisting laboratory studies of interactions of injectable biotherapeutic proteins within the SC environment in relation to bioavailability. We report a new method for directly measuring diffusion of unlabeled, high molecular weight proteins injected into an in vitro matrix that simulates the negatively charged environment of the SC. The matrix consists of 10 mg/ml HA in a repurposed cell culture chamber. The measurement consists of pipetting triplicate 20 µl protein samples into the matrix, placing the chamber in a laboratory scanner, activating tryptophan residues in the protein at 280 nm, and imaging the resulting protein fluorescence at 384 nm over a 0.5–4 h time period thus tracking protein movement. This facile approach enables mapping of protein concentration as a function of time and distance within the matrix, and determination of diffusion coefficients, D, within ±10%. Bovine IgG and BSA gave $D = 2.3 \pm 0.2*10^{-7}$ and $4.6 \pm 0.2*10^{-7}$ cm^2/s at 24°C, respectively, for initial protein concentrations of 21 mg/mL.

KEYWORDS
hyaluronic acid, in vitro assay IgG diffusion, injectable biologics, subcutaneous

1 | INTRODUCTION

There are currently 174 US-approved therapeutic proteins including 98 antibody and biosimilar products and about 560 therapeutic monoclonal antibodies (mAbs) at various stages of research and clinical testing (Rudge & Ladisch, 2020). Subcutaneous (SC) delivery through injection of mAbs is convenient, rapid, and cost-effective, and increases patient compliance and preference with the potential for automated injection (Collins et al., 2017). However, preclinical prediction of systemic mAb diffusion and subsequent absorption from an SC injection site remains challenging.

While blood and lymphatic capillaries are interspersed within the subcutis, uptake of injected mAbs occurs through the lymph capillary network since these proteins (MW of 140–160 kDa) are too large to

pass into the venous system (Mach et al., 2011). Diffusion and the flow of interstitial fluid within the negatively charged extracellular matrix (ECM) carry the protein from injection site to the lymph ducts. In addition to molecular sieving effects due to HA (Laurent et al., 1963), the SC tissue, ECM, and HA behave as a weak cation exchanger. Binding of proteins with pI < pH may occur, although this effect is minimized at high salt (150 mM) or high protein (>30–40 mg/ml) concentrations (Mach et al., 2011; Shenoy & Rosenblatt, 1995). The complex interactions that affect protein transport thus speak to the need for direct measurement of protein diffusion within the HA matrix as is reported here. Other methods measure diffusion by determining concentrations of protein that have passed into the buffer by using SEC, mass spectrometry, and/or spectroscopy (Bown et al., 2018; Leung et al., 2017).

The rate of diffusion of mAbs is subject to other factors including the protein's molecular size, and hydrophobic character as well as viscosity of the formulation of the injected solution. The concentration of hyaluronic acid (HA) is 500 µg/g of skin (or about 1% of collagen). HA is extremely hygroscopic and has a volume potentially 10× that of collagen (Collins et al., 2017; Maharjan et al., 2011; Papakonstantinou et al., 2012). As a first approximation, an in vitro HA matrix simulates key attributes of charge, volume exclusion, and hydrophilic character of the SC region (Bown et al., 2018).

An in vitro method for predicting the bioavailability of SQ injected mAbs was proposed by Bown et al. (2018). In this case, 500 µl of formulated mAb was injected into an SC site simulator (named "Scissors") filled with 6.25 mg/ml HA in PBS solution retained by a dialysis membrane containing small holes through which the protein would diffuse. The concentration of unlabeled protein that diffused into stirred physiologic, carbonate buffer (pH 7.4) was measured over a 4- to 6-h period by SEC (liquid chromatographic) analysis of diluted protein samples carried out offline. The resulting concentration time courses were fitted with the three-parameter Hill equation. Differences between proteins were related to bioavailability and then used to compare the different mAbs.

The development of scissors and a similar approach using agarose gel (Leung et al., 2017) to measure insulin diffusion preceded the current In vitro Subcutaneous Matrix (ISM) system. Diffusion of protein out of agarose gel into buffer was measured through spectral absorbance of protein in buffer. Unlike previous methods, ISM enables in situ measurement of diffusion of concentrated, unlabeled proteins within the HA matrix, itself, and uses smaller sample volumes (20 µl for ISM vs. 500 µl for Scissors). Other advantages of ISM include: flexibility—since user-defined matrices may be placed into the ISM device; throughput—three replicate injections may be made with one device in less than 4 h; and accessibility—ISM leverages existing scanner hardware, present in many laboratories, to determine in situ diffusion of unlabeled protein within ±10%.

The study of diffusion using ISM is based on direct quantification of unlabeled proteins within the matrix. Prior studies have utilized ultraviolet-dependent labeling of proteins with trichloroacetic acid in agarose gels or trichloro ethanol (TCE) incorporated into polyacrylamide gels (Kazmin et al., 2002; Ladner et al., 2004). The

trichloro compounds react with tryptophan upon transillumination at 300 nm for 2–5 min where Trp is present in many proteins (Table 1; Edwards et al., 2002). The labeled fluorescent products are visible to the naked eye and may be captured by camera when protein mass is between 0.2 and 5 µg (Ladner et al., 2004). More recently, Chopra et al. (2019) showed that UV-dependent acylation of both Trp and Tyr residues with TCE (MW 58 Da) results in detectable fluorescence emission at 350–600 nm within 1 mm deep SDS PAGE gels. These reactions are termed as "stain-free" since they avoid staining, rinsing, and de-staining of gels required to image protein bands in electrophoretic gels, but still react label to protein as is the case under some conditions for the Scissors system.

We modified the stain-free approach so that the UV-activated, inherent fluorescence is based on unlabeled protein for the determination of protein mass at depths of up to 6 mm. This is fundamentally different from the concept of stain-free protein detection, where a fixed protein is derivatized in a chemically crosslinked gel. We present methodology for dynamic measurement of mass of unlabeled protein within a viscous HA matrix that simulates the electrostatic environment of the SC region, avoids protein denaturation, and employs a readily available gel scanner that directly determines the distribution of protein mass within a hydrophilic matrix by application of an appropriate standard curve or internal standard.

2 | MATERIALS AND METHODS

2.1 | HA matrix preparation

Sodium hyaluronate (1.5 MDa SH, lot# 028475) powder was purchased from Lifecore Biomedical. Nominal size was 1.5 MDa, with actual size distribution being 1.01–1.8 MDa. Phosphate-buffered saline (PBS) was prepared by combining a 5-L pre-weighed mix (Sigma-Aldrich) with autoclaved deionized water (DI H$_2$O). The HA matrix was prepared by adding 200 mg 1.5 MDa SH to 40 ml PBS (pH 7.4) in a borosilicate glass, round bottom centrifuge tube (DWK Life Sciences), capping the tube, and mixing for 2–4 h at low speed using a Rotisserie Tube Rotator (Scilogex) at room temperature. Addition of a second aliquot of 200 mg 1.5 MDa SH was followed by mixing overnight, and transfer to a refrigerator (4°C) where the formed gel degasses for an additional 24 h, resulting in a clear

TABLE 1 Tryptophan contents of proteins

Protein	Molecular weight (kDa)	% Trp
Lysozyme	14	7.85
α-lactalbumin	14.4	3.2
Trypsin inhibitor	21	1.8
Carbonic Anhydrase	31	4.5
Ovalbumin	45	1.3
BSA	66	0.8
Phosphorylase	1397	2.3

viscous matrix that may be stored at 4°C for up to 2 weeks before use. The HA matrix approximately simulates the viscosity, molecular weight (>1000 kDa), and negatively charged electrostatic environment of SC (Bown et al., 2018; Collins et al., 2017; Cowman et al., 2015; Maharjan et al., 2011; Papakonstantinou et al., 2012).

2.2 | ISM device assembly for measuring in situ protein diffusion in SQ matrices

Diffusion experiments were carried out in a single well chamber (9.40 cm^2 area) while standard curves were obtained with an eight-well chamber slide (0.98 cm^2 area per well; Figure 1a–e). The devices were modified from commercially available clear polycarbonate cell culture chambers (Figure 1c) mounted on borosilicate glass bottoms (76.2 × 25.4 mm^2, NEST Scientific). The UV-opaque borosilicate bottoms were replaced with fused silica (quartz) slides that transmit UV light (required for activation and imaging of proteins; Alfa Aesar). Slides selected for minimal imperfections based on imaging with the BioRad EZ scanner, were re-mounted to the chambers with Loctite superglue (Henkel USA) and cured for 24 h at ambient temperature.

The assembled device was covered by another quartz slide to avoid evaporation of water from the matrix during the course of measurement of up to 4 h in the scanner with antifogging agent (Optix 55) preventing vapor condensation (applied four times at 10-s intervals with a lint-free wipe). After each experiment, HA was removed using DI water, followed by rinsing with 70% ethanol and DI H$_2$O. Each device was reused up to

10 times until the quartz bottom began to lose optical transparency. The combination of commercial off-the-shelf components and reagents, imaging using a commercial gel scanner, and matrix preparation at ambient and refrigerated conditions based on equipment found in a typical wet laboratory speaks to the practicality of the methods reported in this paper.

2.3 | Matrix addition to device

Refrigerated matrix (10 mg HA/ml PBS, 4°C), 660 µl, was transferred from the glass centrifuge tubes to the device using a 1000 µl positive displacement pipette (Mettler-Toledo Rainin) to dispense the HA in a zig-zag pattern so that the gel spreads out into a uniform 6 mm deep matrix upon warming to room temperature. The viscous HA (shear dependent 14 cp at 22°C), once loaded into the single-well, 9.4 cm^2 chamber was covered with the polycarbonate lid provided with the chamber assembly and placed into a humidified plastic container. This allowed the HA matrix to degas while minimizing evaporation from the HA matrix (i.e., <1% in 12 h). The plastic container environment was humidified with water-soaked yellow sorbent pads placed at the bottom of the chamber.

2.4 | Protein standards

Weighed amounts of proteins were dissolved in PBS with 0.05% Tween® 80 (Sigma-Aldrich) and concentrations were determined by
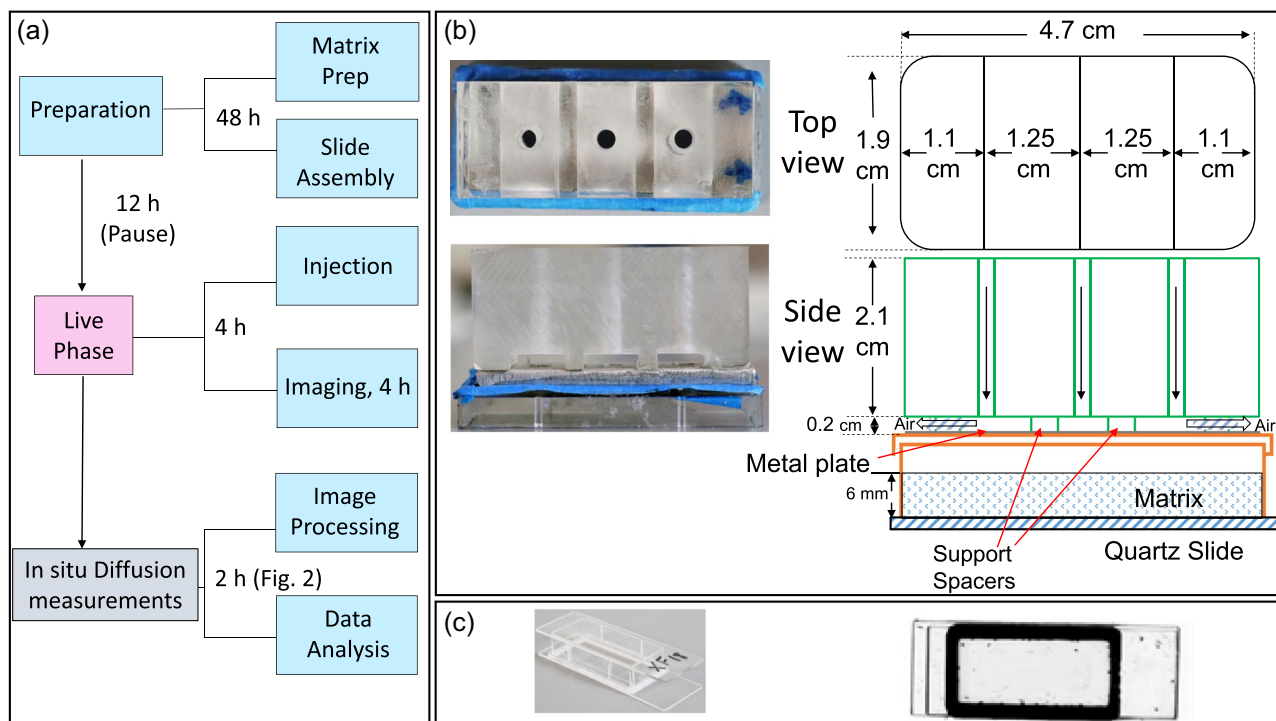

FIGURE 1 Summary of experimental method: (a) workflow; (b) injection guide for introducing protein samples into hyaluronic acid matrices; (c) Side and top views of polycarbonate chamber on quartz slide covered with a second quartz slide on top, before placing it on the tray and inserting into the scanner.

TABLE 2 Properties of proteins examined in this study

Protein	Molecular weight (kDa)	pI	Extinction coefficient (10 mg/ml, 1 cm path)	Zeta potential in PBS pH 7.4 (mV)	Hydrodynamic radius of protein (nm)
BSA	67	4.7	6.7	−8.6 ± 0.1	3.2 ± 0.2
Bovine IgG	150	7	13.7	−2.4 ± 0.1	5.3 ± 0.2

TABLE 3 Protein concentration levels versus total mass for determining standard curves

Protein concentration in PBS + Tween 80	200 µl (2 mm depth)		600 µl (6 mm depth)	
	Total mass (mg)	Mass/pixel (µg)	Total mass (mg)	Mass/pixel (µg)
0	0	0.00	0.0	0.0
7	1.4	0.17	*4.2*	0.50
14	2.8	0.33	*8.4*	1.00
21	*4.2*	0.50	12.6	1.49
28	5.6	0.67	16.8	1.99
35	7.0	0.83	21.0	2.49
42	*8.4*	1.00	25.2	2.99
50	10	1.19	30.0	3.56

extinction coefficients that inherently correct for % moisture (Table 2). BSA, lyophilized powder, ≥96% pure (lot# SLCC9421, Sigma-Aldrich); and IgG from bovine serum (bIgG) ≥95% pure, lyophilized powder (lot# SLBZ8713, Sigma-Aldrich). The proteins were dissolved in 20 ml PBS + Tween 80 in two 1200 mg aliquots (2400 mg protein total) resulting in 120 mg/ml stock solutions in 50 ml, capped centrifuge tubes (Corning Inc.). Dissolution was assisted by inverting the tubes at low speed in the Rotisserie Tube Rotator overnight at room temperature. The tubes were then stored at 4°C for up to 2 weeks until use.

Protein stock solutions were diluted with PBS + Tween 80 to prepare standard solutions (0, 7, 14, 21, 28, 35, 42, and 50 mg/ml) or 50–100 mg/ml samples for diffusion measurements. Concentrations of BSA and bIgG (average of 4 replicates) were measured using 260/280 nm absorbance ratio with Take 3 nanoplates in an Epoch 2 microplate spectrophotometer (US BioTek). Protein size and zeta potential were measured in triplicate using a Zetasizer Nano ZS90 (Malvern Panalytical Inc.) at 1 mg/ml with 1 ml total volume in disposable cuvettes (Thermo Fisher Scientific) pipetted into universal zeta potential dip cell (Malvern Panalytical Inc.). Dilution of the protein standard was with water since Tween 80 and high salt concentrations interfere with Zetasizer measurements by decreasing the overall surface charges and shifting the zeta-potential of proteins toward zero (Salis et al., 2011). Solutions for studying the effects of HA on protein fluorescence were prepared by adding up to 10 mg of 1.5 MDa HA to 1 ml protein solution in PBS + Tween 80, mixing overnight at room temperature in the Rotisserie Tube Rotator at low

speed and refrigerating (4°C) for 24 h in a capped culture tube to degas.

Standard curves for each scanner were determined by placing the cold (4°C) 200 or 600 µl protein solutions, corresponding to 2- or 6-mm sample depths, respectively into the eight-chamber devices using positive displacement pipettes, covering with the quartz slides, equilibrating 30 min to room temperature in the humidified containers and positioning on the "stain-free" tray (part number #1708274, Bio-Rad) for measurement. Concentrations and corresponding mass/pixel values confirmed that this measure of protein mass is independent of matrix depth between 2 and 6 mm (refer to bold and italic values in Table 3).

2.5 | Scanner

We used a pair of instruments (Gel Doc EZ Gel Documentation System #1708270, with Image Lab™ 6.1 software, Bio-Rad; Scanner #1 serial number: 735BR06376 and Scanner #2: 735BR06377) equipped with stain-free trays, on which the devices were placed. Protein was pipetted into an eight-well device (for generating standard curves) or injected into the 9.4 cm² culture chambers containing HA (10 mg/ml) matrix (for diffusion measurements), respectively, and individual devices were placed on each scanner tray at a pre-determined center location using a positioning mask or by aligning with guide marks on the tray.

2.6 | Optical activation/image capture (9.6 cm² chamber)

A 20 µL volume of protein in PBS/Tween 80 was placed into the matrix using the injection guide (Figure 1b). The device (Figure 1c) was placed in the scanner for single-time activation of the protein by the Transillumination UV light (280–300 nm) for 5 min, followed by image capture of the entire tray for 4 s by a camera positioned above the sample. Internal temperature, measured using a type K thermocouple (Omega Engineering) placed an inch away from the device on the tray, showed the lighting within the scanner causes the temperature to increase from 22°C to 25°C during the initial 5 min activation period before stabilizing at 24°C for the remainder of the experiment.

Protein movement through the HA gel was recorded at 30–60 min intervals for up to 4 h without removing the tray from the scanner. The images were subsequently digitally processed to

-WILEY-

correlate protein response to mass. The maximum area imaged by this scanner is $11.2 \times 15\,cm^2$ using a 1.4-MP CCD, at a pixel density of 4096 corresponding to an area of $107.8\,\mu m^2$ per pixel. The signal intensities are the sum of responses of protein molecules in a square column below each pixel. Due to the position of the camera, the samples must be centered in the filter tray to minimize angle distortions of the images.

Imaging of standard solutions utilizes the same methodology except that aliquots of protein either in PBS/Tween 80 or PBS/Tween 80/HA were pipetted into each of the respective wells in the 8-well device and images of each well were processed individually. Total mass/pixel values (Table 3) corresponded to median pixel intensity values for each well with detection limited by the lowest mass per pixel that coincides with system background. Background is due to the combined autofluorescence of scanner tray, glass polycarbonate chamber, quartz cover slide with anti-fog coating, and HA matrix in PBS, and reaches constant intensity within 30 min after the run is started. Tween 80 at 0.05% in buffer increased the background by 198 ± 30. Overall background (=device + HA + Tween 80) was 523 ± 30.

2.7 | Image analysis and concentration mapping (9.4 cm² device)

The images captured by the CCD were converted from scanner format (SCN) to image format (tiff) using Bioformat (Linkert et al., 2010) in MATLAB R2021a (Mathworks). Images were aligned to be vertical in the image coordinate and cropped to include only the region of interest (ROI; Figure 2). The ROI was selected as a rectangle centered in the chamber with boundaries that extend close to inner walls of the chamber while avoiding the projected shadows from the chamber walls due to the scanner lighting system. The cropped ROIs were preprocessed to first remove the outlier pixel intensities caused by dust or air bubbles in the gel. These were identified using a moving median window of 5 by 5 pixels. A 2D Gaussian smoothing function with a standard deviation of 2 pixels was used to suppress noise in the images and determine background autofluorescence (Solomon & Breckon, 2011).

Background intensity was identified as the 45th percentile of the intensity values across the image ROI after 60 min. This represents between 10% and 15% of the maximal signal for the tested proteins. The preprocessed ROIs with protein intensity values (i.e., difference of overall signal and background were converted to protein concentration fields using the standard curves obtained with the eight-well devices (Figure 3). The resulting concentration maps capture the movement of protein mass over time and enabled the calculation of effective diffusion coefficients of proteins within the HA matrix. Variability in mass accounting was 3%–10% for BSA and 1%–4% bIgG for a specific combination of device, tray, and instrument. This approximately doubles if measurements from two different scanners were combined into one data set before image analysis is carried out. Additional statistical analysis was done using MS Excel (Microsoft). Intensity values used to build the standard curve corresponded to the median value of pixels in each ROI.
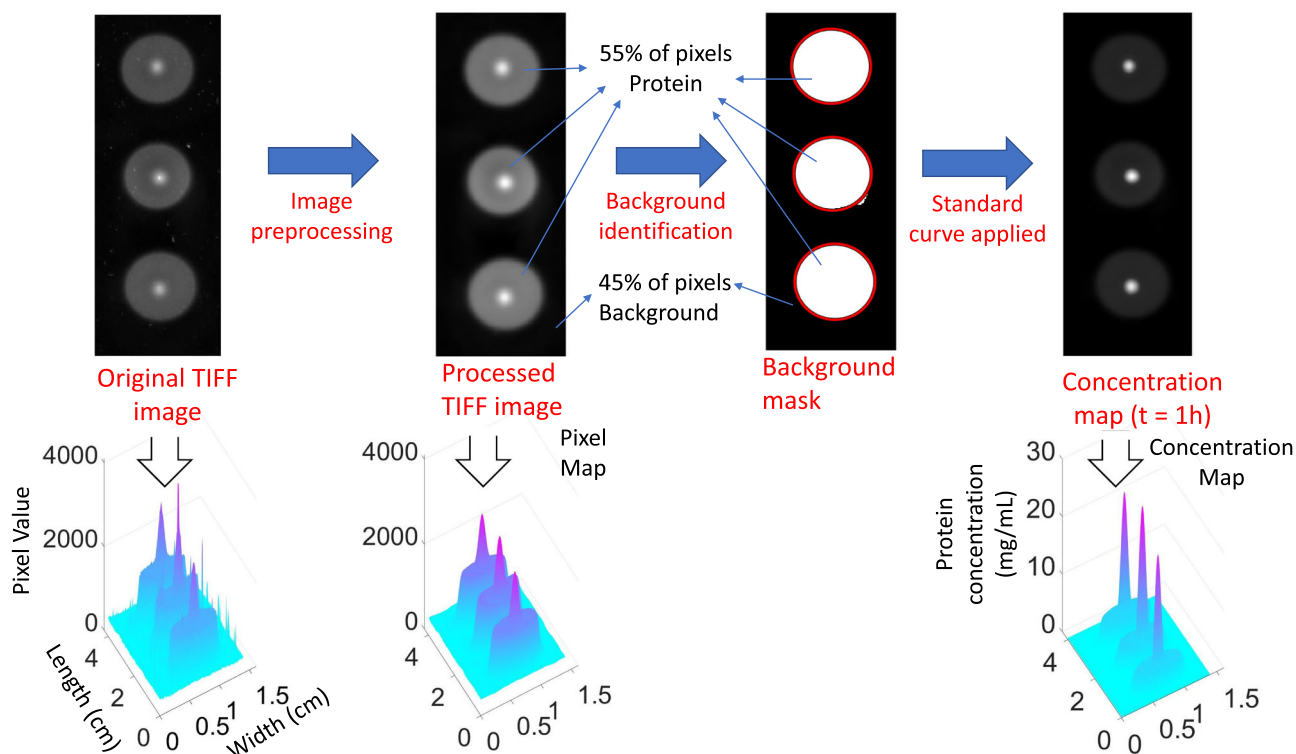

FIGURE 2 Sequence of steps involved in image processing, removing background, and generating concentration map. Image analysis completed within a computational time of 5–20 min.
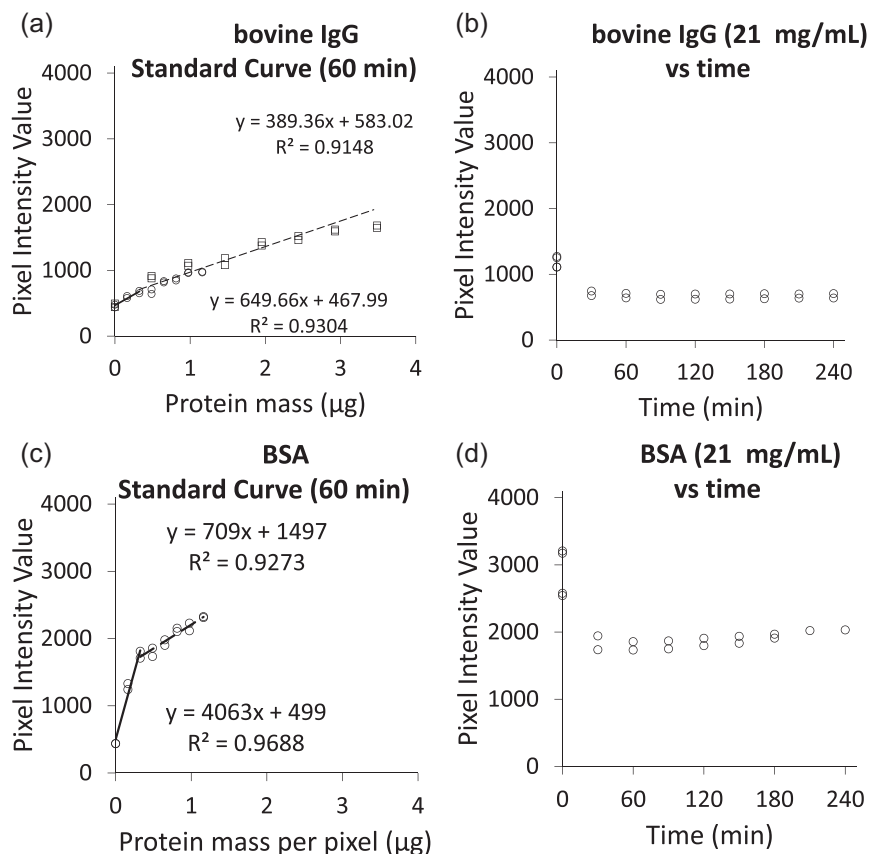
(a) bovine IgG Standard Curve (60 min)

$y = 389.36x + 583.02$
$R^2 = 0.9148$

$y = 649.66x + 467.99$
$R^2 = 0.9304$

Pixel Intensity Value / Protein mass (μg)

(b) bovine IgG (21 mg/mL) vs time

Pixel Intensity Value / Time (min)

(c) BSA Standard Curve (60 min)

$y = 709x + 1497$
$R^2 = 0.9273$

$y = 4063x + 499$
$R^2 = 0.9688$

Pixel Intensity Value / Protein mass per pixel (μg)

(d) BSA (21 mg/mL) vs time

Pixel Intensity Value / Time (min)

FIGURE 3 Standard curves for fluorescent response of unlabeled (a) IgG and (c) BSA showing responses as a function of mass; (b) fluorescent readings stabilize at 30 min after injection for (c) IgG and (d) BSA. Curves in (b) and (d) for protein at an initial concentration of 21 mg/ml.

2.8 | Protein injection into in vitro simulated SC environment

Appropriate injection protocols were necessary to accurately and precisely place concentrated, unlabeled, protein samples at 3 mm depth into the 6 mm deep into viscous, fluidic HA matrix. Interchangeable injection guides placed on top of the single well, 9.40 cm^2 chambers (Figure 1b) were fabricated to enable 20–50 μl protein samples to be inserted at a predetermined depth (3 mm), injection angle (90°), and position (center line of HA matrix). The guides were machined from a 47 × 21 × 19 mm^3 clear cast acrylic (Interstate Plastics) and an aluminum base plate.

This configuration differs from prior literature where protein samples were placed into external channels (i.e., combs) at the top of a 1 mm thick, crosslinked polyacrylamide matrix (Chopra et al., 2019). After movement of the sample into the gel and electrophoresis, the stationary protein bands were reacted with TCE to make them visible (Chopra et al., 2019; Kazmin et al., 2002; Ladner et al., 2004). In our work, spreading of unlabeled protein away from the 3 mm deep injection point was recorded as it occurred for elapsed times of up to 4 h.

2.9 | Pipette tip coating procedure

Injections into the matrix within the chamber must be carried out in a manner that avoids disturbances within, and at the surface of, the HA matrix to minimize initial sample dispersion. Surfaces coated with BSA have reduced interactions with proteins or microorganisms (Huang et al., 2003, 2005, 2006) while non-stick needles utilize metallic glass coating (Chu et al., 2016). Pipette tips were coated with BSA/HA to form a non-stick layer that minimizes disturbances when the pipette tip is inserted into the HA matrix that would obscure protein/matrix boundaries. The three-step coating procedure using a 100 μl positive displacement pipette (Mettler-Toledo Rainin) consisted of (1) loading protein samples (20 μl) into the pipette tip and wiping it with a lint-free wipe; (2) slowly submersing the tip into 10 mg/ml BSA in water solution, submerging for 90 s, removing, and wiping to remove excess BSA leaving a surface coated with protein; (3) inserting the tip into a second tube containing 10 mg/ml HA in PBS for 90 s, removing, and wiping. The coated tip is then inserted through the injection guide and into the matrix.

2.10 | Injections into HA matrix

The coated pipette tip was then inserted through the injection guide placed on a 9.6 cm^2 chamber containing HA matrix (Figure 1b) in a continuous gentle motion lasting about 3 s. Three injections, one per hole, were done in sequence at approximately 1 min intervals. The injection guide was then removed and set aside. An anti-fog-treated quartz slide was placed on the chamber, the chamber was placed on the stain-free tray, and the tray with bubble gauge (to confirm tray

—WILEY—

was kept level) was inserted into the scanner. Activation, imaging, and image processing followed. The protein begins to spread (diffuse) within the HA matrix immediately after each injection. Consequently, start times between the first and third injections differed by 3–5 min before fluorescence for all three protein injections was activated simultaneously at 280 nm. Subsequent image analysis accounted for this time difference to avoid introduction of additional variability.

3 | RESULTS AND DISCUSSION

3.1 | Standard curves and application to image analysis

The standard curves enable the expression of pixel values in terms of protein mass and calibration using internal standards. BSA and bovine IgG standards in PBS/Tween 80, were run in duplicate in the same scanners, at either 2- or 6-mm depths in the eight-well resulting in standard curves at 60 min after activation (Figure 3a,c). The standard curves were used to quantify system response factors, and facilitated the calculation of protein mass as well as to confirm single concentration internal standards could be used in subsequent runs with other proteins. The coefficient of variation of median values of

the duplicate measurements after 60 min was 5.1% for BSA and 7.2% for bIgG within a single scanner. The coefficient of variation when compared across scanners ($n = 4$) was 7.1% for BSA and 5.9% for bIgG. Straight-line fits ($y = mx + b$) resulted in $R^2 > 0.91$ (Figure 3a,c). Intercepts of the lower fitted lines (504 ± 50) represent the combined device and instrument background. The upper fitted lines exhibit decreased slopes due to self-quenching effects from increasing protein mass (Chen & Barkley, 1998) and instrument characteristics. This was particularly pronounced for BSA (Figure 3c), with a median intercept of 1509 ± 143 for the upper fitted line.

The bIgG and BSA standards provided a reference so that small aliquots of other protein samples with known concentrations may be used as two-point internal standards to specify slopes of responses relative to BSA and bIgG. Extinction coefficients allowed protein concentration in standard solutions, before injection, to be independently determined using small (1 μl) samples and are used to calculate protein mass (x-axis in Figure 4). Small sample volumes are important since only limited amounts of concentrated protein are available during the early stages of preclinical testing. Concentrations of internal standards are selected to be above and below an inflection point of 0.47 μg/pixel and below optical saturation (fluorescence intensity of 4095 for this particular model of scanner).
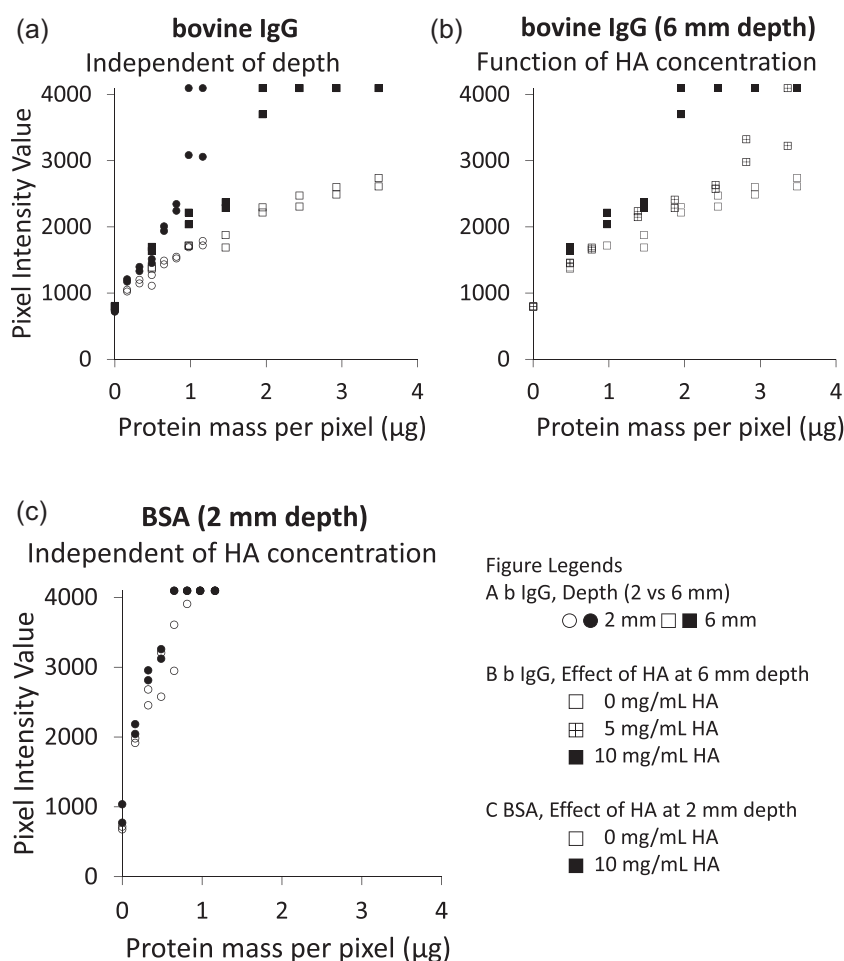

FIGURE 4 Effects of sample depth and hyaluronic acid on protein at long times in eight-well device (a) IgG and in PBS with Tween 80 (open symbols) and with HA added (closed symbols). Results show pixel intensity is independent of sample depth, but is a function of long contact time (36 h) between protein and HA for (b) IgG, but not for (c) BSA. (b) Fluorescent intensity as a function of HA concentrations for IgG in contact with HA for 36 h, 6 mm depth.

3.2 | Effect of HA on fluorescence of unlabeled protein

The fluorescent response of bIgG in PBS/Tween 80 was stable between 30 min and 4 h and 2- and 6-mm depths (example in Figure 3b,d for protein at 21 mg/ml). Figure 4a shows that fluorescent response is independent of depth between 2 mm (open circles) and 6 mm (open boxes) for bIgG both in the presence and absence of HA. When bIgG was incubated with added HA at 10 mg/ml for 36 h, before injection (≈12 h mixing with HA at ambient temperature and 24 h degassing in the refrigerator at 4°C) a twofold increase in fluorescence intensity occurred at an HA:protein ratio of 2 (Figure 4b). The difference in intensities increased with increasing HA from 0 to 10 mg/ml (Figure 4b). BSA incubated with no HA and in 10 mg/ml HA added gave similar intensities after 36 h (Figure 4c).

Counteracting effects in an HA matrix whose pH (7.4) is close to bIgG's isoelectric point but removed from the pI (4.7) for BSA (Table 2) help to explain the enhanced response of IgG after long (36 h) contact with HA, and are associated with fluorescent quenching or enhancement effects. Since pI≈pH for IgG, protein instability is expected, while BSA (pI 4.7) would not be affected. Enhancement of fluorescence through proximity or orientation of glutamine, asparagine, glutamic and aspartic acids, cysteine, and histidine side chains by excited electron transfer, and tyrosine and lysine by excited state proton transfer is known to contribute to fluorescent response and cause shifts in absorption and/or emission wavelengths (Chen & Barkley, 1998; Johansson, 1997; Vivian & Callis, 2001).

3.3 | Selection of run conditions

The overall results informed selection of run times (i.e., 30 min to 4 h), mass ranges (Table 3), concentrations of single-point internal

standards for known masses of test proteins, and confirmation that measurement of protein on a mass basis is independent of matrix depths at between 2 and 6 mm. In addition, reproducible injections did not require premixing the protein with HA (Figure 2) thus simplifying the assay.

3.4 | Protein mass balance in an HA matrix

Calibration curves (Figure 3a,c) facilitate the correlation of protein mass to fluorescence and observation of the behavior of unlabeled protein at high concentrations in an HA matrix (Figure 2). Six 20 µl injections (three per chamber, Figure 1a for bIgG or BSA followed by imaging over 4 h and mapping of the images using standard curves, enabled protein mass to be accounted for based on response above background with 90%–99% of BSA (Figure 5b) and 60%–70% of IgG accounted for (Figure 5a). IgG has a lower response than BSA (compare Figure 3a–c), and the IgG at the outer edge approaches detection limits, resulting in a smaller difference between signal and background and a lower measured extent of mass recovery within the limits of the E-Z scanner. Increased resolution in a new model (Bio-Rad Gel Doc Go Imaging System) results in a larger difference between background and signal with preliminary data indicating this is sufficient to obtain closure of the protein mass balance of IgG as well (unpublished data).

3.5 | Diffusion

An initial estimate of the diffusion coefficient, D (cm^2/s) is calculated from $D = (d_t - d_o)^2/(32 (t - t_o))$, assuming an isotropic matrix and constant diffusion (Cushman-Roisin, 2012), where d_t and d_0 are the diameters of the area occupied by the protein (cm) at t_o and t (s) representing elapsed times of 1 and 4 h (i.e., 3600 and 14,400 s),
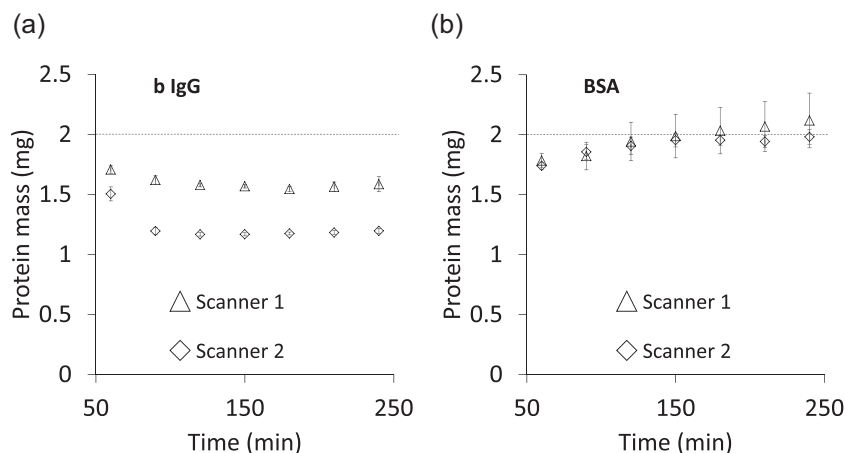

FIGURE 5 Calculated mass recovery from standard curves and image analysis (triangles and diamonds) for (a) IgG and (b) BSA compared to known mass of injected protein (20 µl, 2 mg, $n = 6$, dotted line). Runs carried out in two separate scanners. Scanner #1 serial number 735BR06376 (open triangles) and Scanner #2 735BR06377 (open diamonds), respectively, with scanner 1, which was more heavily used, giving an attenuated response (intensity of light source decreases over time) compared to Scanner 2. This difference results in a smaller signal-to-noise ratio and a lower accounting of the fraction of protein mass that is below the detection threshold for this particular instrument. Injected protein mass measured separately using extinction coefficients (spectrophotometric assay).

respectively, after injection. D for IgG or BSA in a 10 mg/ml HA matrix at 24°C gave averaged values of $(2.3 \pm 0.2)*10^{-7}$ cm^2/s for IgG and $(4.6 \pm 0.2)*10^{-7}$ cm^2/s for BSA with both proteins initially at 21 mg/ml. This compares to reported values of 4.0 and $5.9*10^{-7}$ cm^2/s for IgG and BSA, respectively, in free solution (Hennink et al., 1996), and 4.52 or $3.2*10^{-7}$ cm^2/s for BSA in 25 and 30 mg/ml HA, respectively (Shenoy & Rosenblatt, 1995). These values are within the expected ranges. Further analysis and modeling of the diffusion profiles are needed and underway to account for the concentration dependence of protein diffusion (Saluja et al., 2010), and to test mAbs. Once validated with other proteins, the utility of this tool is anticipated to be in testing for the differentiation of drug candidates, characterization of critical property attributes, and provision of a physicochemical model anticipating a clinical attribute. Additional work is necessary (and underway) for this method to attain a level of maturity suitable for broader applications.

4 | CONCLUSIONS

Label-free protein standards enabled mapping of mass as a function of fluorescence intensities of unlabeled proteins within a 6 mm deep HA matrix that simulates the electrostatic environment of the SC region. The developed protocols, carried out over a 30 min to 4 h time period, facilitated interrogation of behaviors of high molecular weight concentrated proteins within a viscous, charged matrix. Once standard curves are established—in our case these were for BSA (MW 67 kDa, pI 4.7) and bIgG (MW 150 kDa, pI 7.0)—the resulting calibrations were applied to the analysis of images of protein spreading patterns. The resulting maps of injected protein mass as a function of time illustrate concepts by which protein behavior in the SC region and diffusion coefficients may be inferred based on in vitro measurements. This approach has utility for comparing in vitro to in vivo behavior of IgG type mAbs and providing data to model protein diffusion within a matrix that simulates the SQ environment.

AUTHOR CONTRIBUTIONS

Antonio C. F. dos Santos: Writing–review and editing, investigation, methodology, interpretation of data, validation, formal analysis, visualization, data curation. **Adib Ahmadzadegan**: Formal analysis, visualization, interpretation. **Eduardo Ximenes**: Methodology, interpretation, analysis. **Pavlos Vlachos**: Formal analysis, interpretation of data, investigation, methodology. **Arezoo Ardekani**: Formal analysis, interpretation of data. **Shiven Kapur**: Writing–review and editing, formal analysis, interpretation of data. **Vince Corvari**: Conceptualization, interpretation, formal analysis. **Michael Ladisch**: Conceptualization, formal analysis, supervision, methodology, writing–review and editing, interpretation of data, resources, visualization.

DATA AVAILABILITY STATEMENT

The data that support the findings of this study are available on request from the corresponding author.

ORCID

Antonio C. F. dos Santos 🄳 https://orcid.org/0000-0002-7389-2463
Michael R. Ladisch 🄳 https://orcid.org/0000-0001-9953-9599

REFERENCES

Bown, H. K., Bonn, C., Yohe, S., Yadav, D. B., Patapoff, T. W., Daugherty, A., & Mrsny, R. J. (2018). *In vitro* model for predicting bioavailability of subcutaneously injected monoclonal antibodies. *Journal of Controlled Release*, 273, 13–20. https://doi.org/10.1016/j.jconrel.2018.01.015

Chen, Y., & Barkley, M. D. (1998). Toward understanding tryptophan fluorescence in proteins. *Biochemistry*, 37, 9976–9982. https://doi.org/10.1021/bi980274n

Chopra, A., Willmore, W. G., & Biggar, K. K. (2019). Protein quantification and visualization via ultraviolet-dependent labeling with 2, 2, 2-trichloroethanol. *Scientific Reports*, 9(1):13923. https://doi.org/10.1038/s41598-019-50385-9

Chu, J. P., Yu, C. C., Tanatsugu, Y., Yasuzawa, M., & Shen, Y. L. (2016). Non-stick syringe needles: beneficial effects of thin film metallic glass coating. *Scientific Reports*, 6(1), 31847. https://doi.org/10.1038/srep31847

Collins, D. S., Kourtis, L. C., Thyagarajapuram, N. R., Sirkar, R., Kapur, S., Harrison, M. W., Bryan, D.J., Jones, G.B., & Wright, J.M. (2017). Optimizing the bioavailability of subcutaneously administered biotherapeutics through mechanochemical drivers. *Pharmaceutical Research*, 34(10), 2000–2011. https://doi.org/10.1007/s11095-017-2229-9

Cowman, M. K., Schmidt, T. A., Raghavan, P., & Stecco, A. (2015). Viscoelastic properties of hyaluronan in physiological conditions. *F1000 Research*, 4, 622. https://doi.org/10.12688/f1000research.6885.1

Cushman-Roisin, B. (2012). Dartmouth College, Environmental Transport and Fate, Chapter 2 Lecture notes, page (with permission), pp. 25–72.

Edwards, R. A., Jickling, G., & Turner, R. J. (2002). The light-induced reactions of tryptophan with halo compounds. *Photochemistry and Photobiology*, 75(4), 362–368. https://doi.org/10.1562/0031-8655(2002)075%3C0362:TLIROT%3E2.0.CO;2

Hennink, W. E., Talsma, H., Borchert, J. C. H., De Smedt, S. C., & Demeester, J. (1996). Controlled release of proteins from dextran hydrogels. *Journal of Controlled Release*, 39(1), 47–55. https://doi.org/10.1016/0168-3659(95)00132-8

Huang, T.T., Sturgis, J., Gomez, R., Geng, T., Bashir, R., Bhunia, A. K., Robinson, J. P., & Ladisch, M. R. (2003). Composite surface for blocking bacterial adsorption on protein biochips. *Biotechnology and Bioengineering*, 81(5), 618–624. https://doi.org/10.1002/bit.10507

Huang, T.T., Taylor, D. G., Lim, K-S., Sedlak, M., Bashir, R., Mosier, N. S., & Ladisch, M. R. (2006). Surface-directed boundary flow in microfluidic channels. *Langmuir*, 22(14), 6429–6437. https://doi.org/10.1021/la053465h

Huang, T.T., Taylor, D. G., Sedlak, M., Mosier, N. S., & Ladisch, M. R. (2005). Microfiber-directed boundary flow in press-fit microdevices fabricated from self-adhesive hydrophobic surfaces. *Analytical Chemistry*, 77(11), 3671–3675. https://doi.org/10.1021/ac048228i

Johansson, J. S. (1997). Binding of the volatile anesthetic chloroform to albumin demonstrated using tryptophan fluorescence quenching. *Journal of Biological Chemistry*, 272, 17961–17965. https://doi.org/10.1074/jbc.272.29.17961

Kazmin, D., Edwards, R. A., Turner, R. J., Larson, E., & Starkey, J. (2002). Visualization of proteins in acrylamide gels using ultraviolet illumination. *Analytical Biochemistry*, 301(1), 91–96. https://doi.org/10.1006/abio.2001.5488

Ladner, C.L., Yang, J., Turner, R. J., & Edwards, R. A. (2004). Visible fluorescent detection of proteins in polyacrylamide gels without staining. *Analytical Biochemistry*, 326, 13–20. https://doi.org/10.1016/j.ab.2003.10.047

Laurent, T. C., Björk, I., Pietruszkiewicz, A., & Persson, H. (1963). On the interaction between polysaccharides and other macromolecules. *Biochimica et Biophysica Acta*, 78(2), 351–359. https://doi.org/10.1016/0006-3002(63)91645-7

Leung, D. H., Kapoor, Y., Alleyne, C., Walsh, E., Leithead, A., Habulihaz, B., Salituro, G.M., Bak, A., & Rhodes, T. (2017). Development of a convenient in vitro gel diffusion model for predicting the in vivo performance of subcutaneous parenteral formulations of large and small molecules. *AAPS PharmSciTech*, 18(6), 2203–2213. https://doi.org/10.1208/s12249-016-0698-5

Linkert, M., Rueden, C. T., Allan, C., Burel, J-M., Moore, W., Patterson, A., Loranger, B., Moore, J., Neves, C., MacDonald, D., Tarkowska, A., Sticco, C., Hill, E., Rossner, M., Eliceiri, K. W., & Swedlow, J. R. (2010). Metadata matters: Access to image data in the real world. *Journal of Cell Biology*, 189(5), 777–782. https://doi.org/10.1083/jcb.201004104

Mach, H., Gregory, S. M., Mackiewicz, A., Mittal, S., Lalloo, A., Kirchmeier, M., & Shameem, M. (2011). Electrostatic interactions of monoclonal antibodies with subcutaneous tissue. *Therapeutic Delivery*, 2(6), 727–736. https://doi.org/10.4155/tde.11.31

Maharjan, A. S., Pilling, D., & Gomer, R. H. (2011). High and low molecular weight hyaluronic acid differentially regulate human fibrocyte differentiation. *PLoS One*, 6(10):e26078. https://doi.org/10.1371/journal.pone.0026078

Papakonstantinou, E., Roth, M., & Karakiulakis, G. (2012). Hyaluronic acid: A key molecule in skin aging. *Dermato-Endocrinology*, 4(3), 253–258. https://doi.org/10.4161/derm.21923

Rudge, S. R., & Ladisch, M. R. (2020). Industrial challenges of recombinant proteins, *Current applications of pharmaceutical biotechnology*. Advances in biochemical engineering/biotechnology (Vol. 171, pp. 1–22). Springer.

Salis, A., Boström, M., Medda, L., Cugia, F., Barse, B., Parsons, D. F., Ninham, B.W., & Monduzzi, M. (2011). Measurements and theoretical interpretation of points of zero charge/potential of BSA protein. *Langmuir*, 27(18), 11597–11604. https://doi.org/10.1021/la2024605

Saluja, A., Fesinmeyer, R. M., Hogan, S., Brems, D. N., & Gokarn, Y. R. (2010). Diffusion and sedimentation interaction parameters for measuring the second virial coefficient and their utility as predictors of protein aggregation. *Biophysical Journal*, 99(8), 2657–2665. https://doi.org/10.1016/j.bpj.2010.08.020

Shenoy, V., & Rosenblatt, J. (1995). Diffusion of macromolecules in collagen and hyaluronic acid, rigid-rod-flexible polymer, composite matrixes. *Macromolecules*, 28(26), 8751–8758. https://doi.org/10.1021/ma00130a007

Solomon, C., & Breckon, T. (2011). *Fundamentals of digital image processing: A practical approach with examples in Matlab* (p. 354). John Wiley & Sons, Wiley-Blackwell.

Vivian, J. T., & Callis, P. R. (2001). Mechanisms of tryptophan fluorescence shifts in proteins. *Biophysical Journal*, 80(5), 2093–2109. https://doi.org/10.1016/S0006-3495(01)76183-8

SUPPORTING INFORMATION

Additional supporting information can be found online in the Supporting Information section at the end of this article.

How to cite this article: dos Santos, A. C. F., Ahmadzadegan, A., Ximenes, E., Vlachos, P., Ardekani, A., Kapur, S., Corvari, V., & Ladisch, M. R. (2022). In vitro measurement of concentration of unlabeled protein within a hyaluronic acid matrix. *Biotechnology and Bioengineering*, 119, 3647–3656. https://doi.org/10.1002/bit.28243